IHJPAS. 36 (4) 2023

Ibn Al-Haitham Journal for Pure and Applied Sciences
Journal homepage: jih.uobaghdad.edu.iq

The Gas Sensitivity Properties of Nano Ferrite $Cu_xAl_{0.3-X}Ni_{0.7}Fe_2O_4$ Synthesized by Sol-Gel Method

Shaymaa A. Kadhim *
Department of phesics, College of Education for Pure Sciences, Ibn Al-Haitham University of Baghdad, Iraq

Tagreed M. Al- Saadi
Department of Phesics, College of Education for Pure Sciences, Ibn Al-Haitham University of Baghdad, Iraq

***Corresponding Author:** Shaimaa.Ahmed1104a@ihcoedu.uobaghdad.edu.iq

Article history: Received 28 November 2022, Accepted 18 January 2023, Published in October 2023

doi.org/10.30526/36.4.3118

Abstract:
This study includes the preparation of the ferrite nano ferrite $Cu_xAl_{0.3-X}Ni_{0.7}Fe_2O_4$ (where: x = 0, 0.05, 0.1, 0.15, 0.2, 0.25, 0.3) M using the auto combustion method (sol-gel), and citric acid was used as fuel for auto combustion. The ferrite samples were checked by X-ray diffraction (XRD), Field Emission Scanning Electron Microscopes (FE-SEM), and energy dispersive X-ray analyzer (EDX). They showed that the prepared compound has a face-centered cubic structure (FCC). The lattice constant increases with an increase in the percentage of doping of the copper ions, and a decrease for the aluminum ion and that the compound is porous and its grains are spherical, and there are no other elements other than the elements involved in the preparation of the compound. Which means that it is of high purity. The gas sensing system revealed that the nano ferrite has good sensitivity to hydrogen sulfide (H_2S) gas.

Keywords: nano ferrite, H_2S gas, sensitivity, Response time, Recovery time.

1. Introduction

$NiFe_2O_4$ ferrite is a material that can be found in many electronic components, such as capacitors and inductors. It has a high magnetic permeability, which makes it an excellent choice for applications that require a lot of magnetism or static electricity, such as transformers and motors. It can also be used to reduce high-frequency noise in electronics by acting as a barrier. It is also used as a detector for many gases and humidity. A very poisonous and flammable gas with detrimental effects on human health and the environment is hydrogen sulfide. This gas may not

be present in the atmosphere in excess of 10 ppm. Therefore, it's crucial to create sensors that can recognize low H_2S concentrations [1]. The popularity of semiconductor-based chemical sensors is due to their compact size, straightforward operation, high sensitivity, selectivity, and reasonably straightforward auxiliary electronics [2]. However, when detecting a target gas from a mixture of gases, the lack of selectivity is a disadvantage. Doping with various materials is one of the most common ways to increase sensor selectivity and sensitivity [3, 4]. The use of several distinct semiconductor oxides as sensing components for gas sensing in bulk ceramics, thick films, and thin-film forms has been studied [5]. As an alternative material, spinel ferrites have been used in the gas sensor industry. Several sensors will be taken into consideration before concentrating on ferrites as gas sensors, their crystal structure, and production methods. Gas sensors work by detecting changes in a material's electrical, acoustic, optical, mass, or calorimetric properties. The most focus is being paid to detection based on differences in electrical properties since it is easy, rapid, and affordable. The requirement for sensors to be included into smart devices for remote sensing is growing, and portability and operating system compatibility are accelerating the development of electrical detection-based sensors [6]. Semiconducting oxygenizes MFe_2O_4 spinel semiconductors have been identified as a sensitive formula. Materials react with both oxidizing and reducing gases [7]. Researchers are interested in nano-ferrites because of their easily adaptable features and wide range of potential applications in sensors, microwave devices, etc... For the cation site in the spinel ferrite structure of gas sensors, hundreds of metal oxide materials are used as active layers as thick or incredibly thin films. The structure of spinel is composed of 32 oxygen atoms organized in a cubic crystal system with 64 tetrahedral sites. Chemical control, home security, and environmental monitoring can all benefit from 32-site octahedral gas sensors. More innovative materials are being created for high-performance solid-state gas sensors [8]. The Fe-Fe reactions affect the ferrite's structural, electrical, and magnetic characteristics [9]. Finally, the purpose of this work is to investigate the effect of replacing Al ion with Cu on the structural and sensitivity to H_2S gas features of (sol-gel) generated ferrite nanoparticles $Cu_xAl_{0.3-X}Ni_{0.7}Fe_2O_4$.

2. Experimental

To prepare the raw components for use, the auto combustion (sol-gel) technique was used. $Cu_xAl_{0.3-X}Ni_{0.7}Fe_2O_4$. Table 1 outlines the substances obtained.

Table 1. Masses of raw materials used in the preparation of nano ferrite $Cu_xAl_{0.3-x}Ni_{0.7}Fe_2O_4$.

citric acid		aluminum nitrate		copper nitrate		nickel nitrate		iron nitrate	
n	m(g)	$n_{0.3-x}$	m(g)	n_x	m(g)	n	m(g)	n	m(g)
3	23.0556	0.3	4.50156	0	0	0.7	8.14268	2	32.32
3	23.0556	0.25	3.7513	0.05	0.4832	0.7	8.14268	2	32.32
3	23.0556	0.2	3.00104	0.1	0.9664	0.7	8.14268	2	32.32
3	23.0556	0.15	2.25078	0.15	1.4496	0.7	8.14268	2	32.32
3	23.0556	0.1	1.50052	0.2	1.9328	0.7	8.14268	2	32.32
3	23.0556	0.05	0.75026	0.25	2.416	0.7	8.14268	2	32.32
3	23.0556	0	0	0.3	2.8992	0.7	8.14268	2	32.32

Firstly, the metal nitrate was added to a 1000 mL heat-resistant glass beaker. We add citric acid to a separate beaker, followed by (40 ml) of deionized water, and then added the acid solution to the Nitrate solution. Using a magnetic stirring device, the two solutions are fully combined

without heating, and then a small amount of ammonia in the form of drops is added to the mixture until the pH is equalized (7). After that, the magnetic stirrer heater was turned on until the temperature of the mixture reaches (90 0C). The mixing process continued with heating until the mixture became a gel, and then the mixer motor is stopped while the heating continues until the gel ignites automatically, and completely. Then the resulting ferrite left to cool and then grind it with a mortar, and then we put the resulting ferrite powder inside the oven for two hours at a time for each sample. The structural properties of the resulting ferrite powder are then investigated using XRD, FE-SEM, and EDX techniques. Following the aforementioned measurements, 1.5 g of the powder from each sample was collected and manually pressed for one minute at 200 bar pressure, resulting in a disc with a diameter of 1 cm and a thickness of 3.5 mm for each sample. Seven samples were produced for the prepared ferrite. Then the samples were placed in the oven for two hours at 900°C. The gas sensitivity method was then used to create electrodes for each sample and determine their sensitivity to H_2S gas.

3. Results and Discussion:

3.1. X-Ray Diffraction:

Figure (1) shows the X-ray diffraction patterns of $Cu_xA_{0.3-X}Ni_{0.7}Fe_2O_4$ ferrite nanocomposite samples compared to the $NiFe_2O_4$ diffraction plot in JCPDS Standard Card No. 10-0325.

The X-ray diffraction patterns of the prepared compound samples show that there are more than seven clear peaks within the range (200-800) belonging to the surfaces: (111), (220), (311), (400), (422), (511), (440), and the apparent peaks indicate the nature of the crystal structure of the prepared compound's ferrite powder, which was of the face-centered cubic spinel type (FCC) [10].

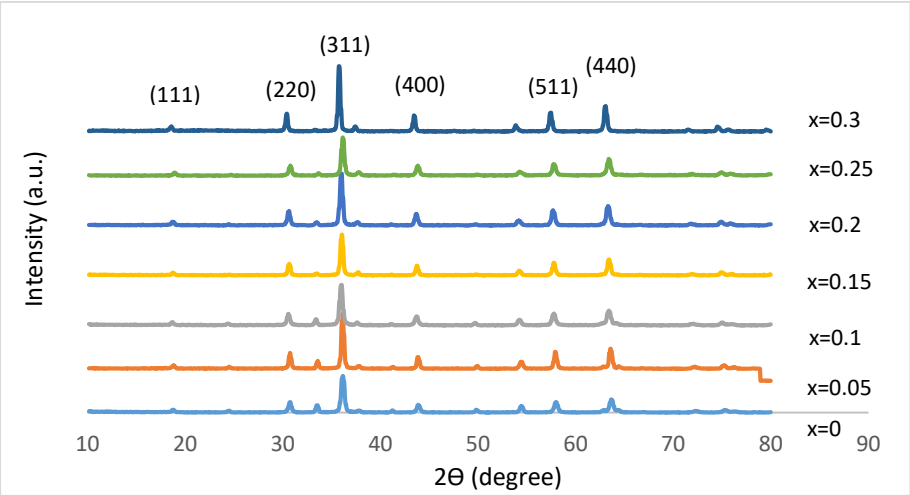

Figure 1. The X-ray diffraction patterns of $Cu_xAl_{0.3-X}Ni_{0.7}Fe_2O_4$ ferrite nanoparticles samples.

"Fullprof suit software" was used to determine the lattice parameters, and "The Scherer equation" [11, 12] was used to calculate the crystallite size.

$$D_{Sh} = K\,\lambda / \beta \cos\theta \qquad (1)$$

Where: λ the wavelength of X-ray (1.54 Å), β is full width at half maximum, and θ the incident angle.

Table 2. Lattice constants (lattice constant, crystallite size and density).

Cu Content (mole)	Lattice constant (Å)	Crystallite size (nm)	Density (g/cm^3)
0	8.29027	34.30426151	5.398
0.05	8.30641	31.89985964	5.367
0.1	8.31565	34.30426151	5.349
0.15	8.32698	29.80296574	5.327
0.2	8.33509	35.22717507	5.311
0.25	8.35207	26.41396643	5.279
0.3	8.35432	33.20924561	5.275

With the exception of one reading in **Table (2)** it can be seen that the lattice constant rises as the percentage of copper ion increases by comparing the results in **Table (2)** with the molar concentrations of copper ion (x = 0, 0.05, 0.1, 0.15, 0.2, 0.25, 0.3). Because of the migration of iron cations Fe^{+3} from the quaternary spaces to the eight spaces to be replaced by impurity cations and the enlargement of the quaternary spaces as a result of the added impurities, the addition of dopants and their increasing ratio boosts the value of the lattice constant [13], and the reconstruction of the surface has an impact on the lattice constant, changing its value. This shift in the lattice constant value is particularly significant in nanocrystals since they have a high surface area to volume ratio [14], this shift in the lattice constant implies that alternative ions entered the crystal system in a substitution or interstitial way between the iron ions, resulting in the lattice widening and a fall in the density value, which can also be attributed to added impurities [15].

3.2. SEM and EDX Analysis

In order to clearly specify the nature of the surface and form of the particles as well as their rate of grain size, samples of the produced compound ($Cu_xAl_{0.3-X}Ni_{0.7}Fe_2O_4$) were photographed using the emission field scanning electron microscopy (FE-SEM) technique. **Figure (2)** shows that the substance is indeed in the nanometer range and has been verified to be in that range. The nanoparticles of the samples of the mentioned substance are spherical or semi-spherical in shape with the presence of some gatherings or agglomerations. There are also voids between the region's conglomerates or agglomerations, and these voids represent the porous nature of the surface of the substance, which is necessary for gas adsorption [16], and the presence of holes is produced by the presence of impurities, which advances the value of the crystal lattice constant and hence increases the specific surface area in relation to the volume of the compound. As a result of the foregoing, a porous structure is formed, which improves the sensor's response to the test gas [17].

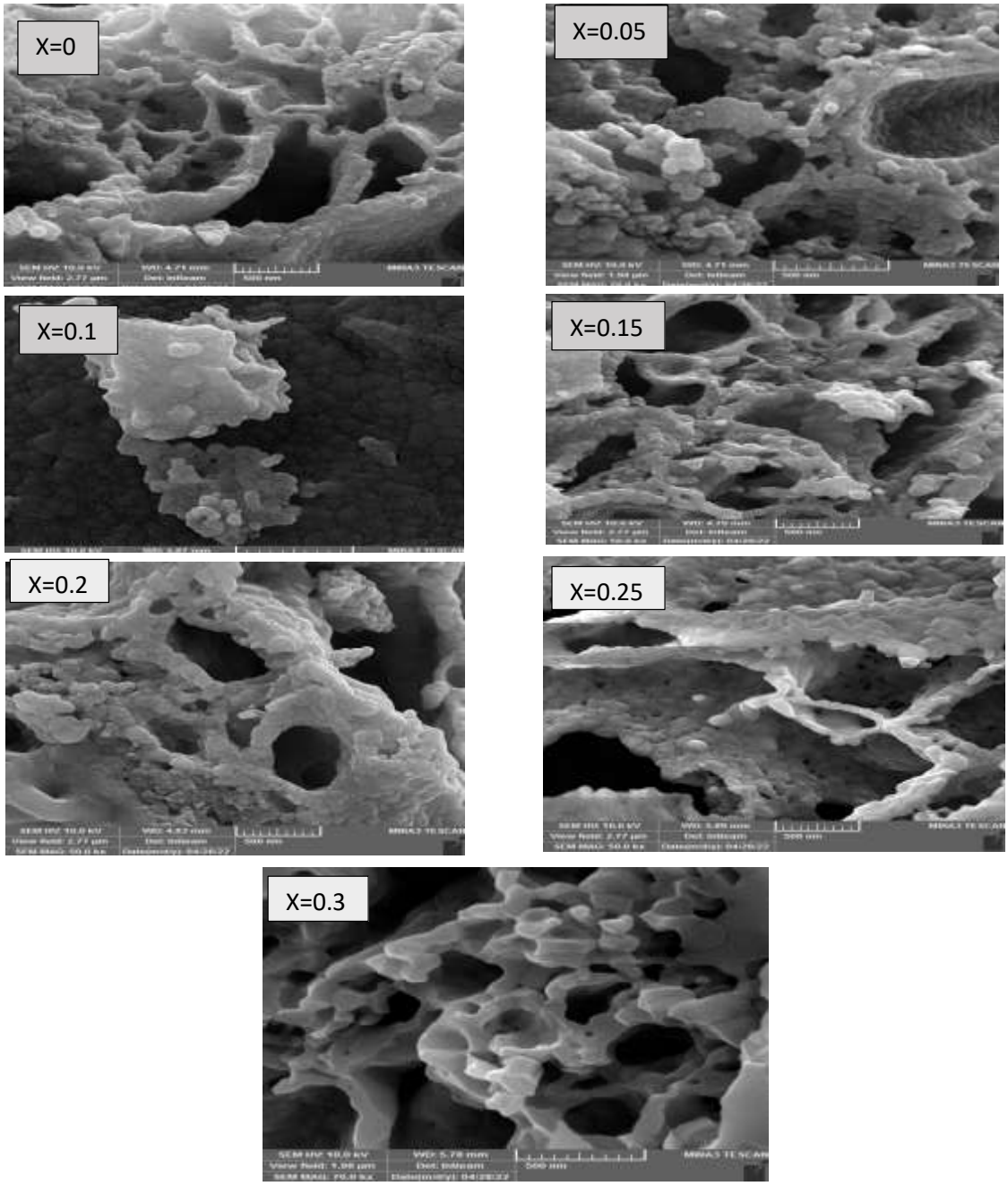

Figure 2. FE-SEM images of the $Cu_xAl_{0.3-x}Ni_{0.7}Fe_2O_4$ ferrite nanoparticles samples.

As shown in **Figure (3)** and **Table (3),** the Energy-dispersive X-ray spectroscopy (EDS) and emitting field scanning electron microscope (FE-SEM) were used to confirm the presence of the components of the prepared compound ($Cu_xAl_{0.3-x}Ni_{0.7}Fe_2O_4$). It is clear from the images that all the elements that formed the nano-ferrite are present, that means all samples are pure and free from impurities.

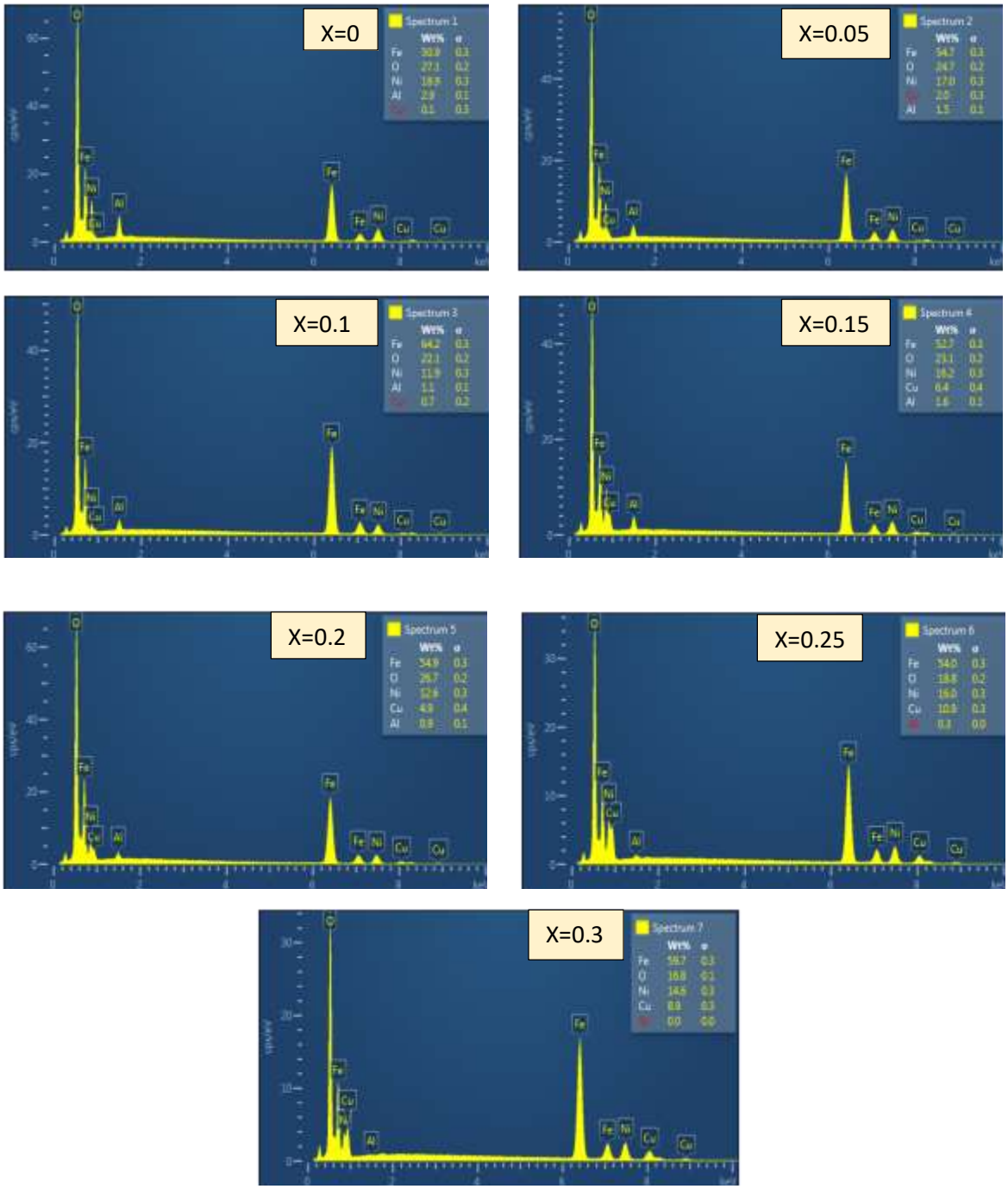

Figure 3. EDX images of the ferrite nanoparticles samples $Cu_xAl_{0.3-x}Ni_{0.7}Fe_2O_4$

Table 3.The atomic and weight ratios of the $Cu_xAl_{0.3-x}Ni_{0.7}Fe_2O_4$ nano ferrite elements.

X=0

Element	Line Type	Atomic %	Wt %
O	K series	55.77	27.12
Fe	K series	29.99	50.92
Ni	K series	10.61	18.93
Cu	L series	0.05	0.09
Al	K series	3.58	2.94
Total		100.00	100.00

X=0.05

Element	Line Type	Atomic %	Wt %
O	K series	53.25	24.74
Fe	K series	33.75	54.74
Ni	K series	0.30	17.02
Cu	L series	1.07	1.98
Al	K series	1.95	1.53
Total		100.00	100.00

X=0.1

Element	Line Type	Atomic %	Wt %
O	K series	49061	22.12
Fe	K series	41.21	64.15
Ni	K series	7.27	11.89
Cu	L series	0.39	0.69
Al	K series	1051	1.14
Total		100.00	100.00

X=0.15

Element	Line Type	Atomic %	Wt %
O	K series	51.16	23.12
Fe	K series	33.38	52.66
Ni	K series	9.76	16.18
Cu	L series	3.59	4.66
Al	K series	2.11	1.61
Total		100.00	100.00

X=0.2

Element	Line Type	Atomic %	Wt %
O	K series	56.05	26.68
Fe	K series	33.06	54.94
Ni	K series	7.20	12.58
Cu	L series	2.61	4.93
Al	K series	1.08	0.87
Total		100.00	100.00

X=0.25

Element	Line Type	Atomic %	Wt %
O	K series	45.26	18.81
Fe	K series	37.26	54.05
Ni	K series	10.50	16.01
Cu	L series	6.27	10.85
Al	K series	0.41	0.28
Total		100.00	100.00

X=0.3

Element	Line Type	Atomic %	Wt %
O	K series	41.82	16.78
Fe	K series	42	59.68
Ni	K series	9.91	14.59
Cu	L series	5.61	8.94
Al	K series	0.02	0.02
Total		100.00	100.00

3.3. Sensing properties:

Equation (2) [18] was used to compute the $Cu_xAl_{0.3-x}Ni_{0.7}Fe_2O_4$ samples' sensitivity to Hydrogen sulfide gas (H_2S), and the findings revealed that the sensitivity to H_2S gas changes as the operating temperature changes, as shown in Figure (4).

$$S = (|Ra- Rg|/Ra)*100\% \quad (2)$$

Where: Ra the sensor model's electrical resistance in air, Rg the gas-sensitive model's electrical resistance.

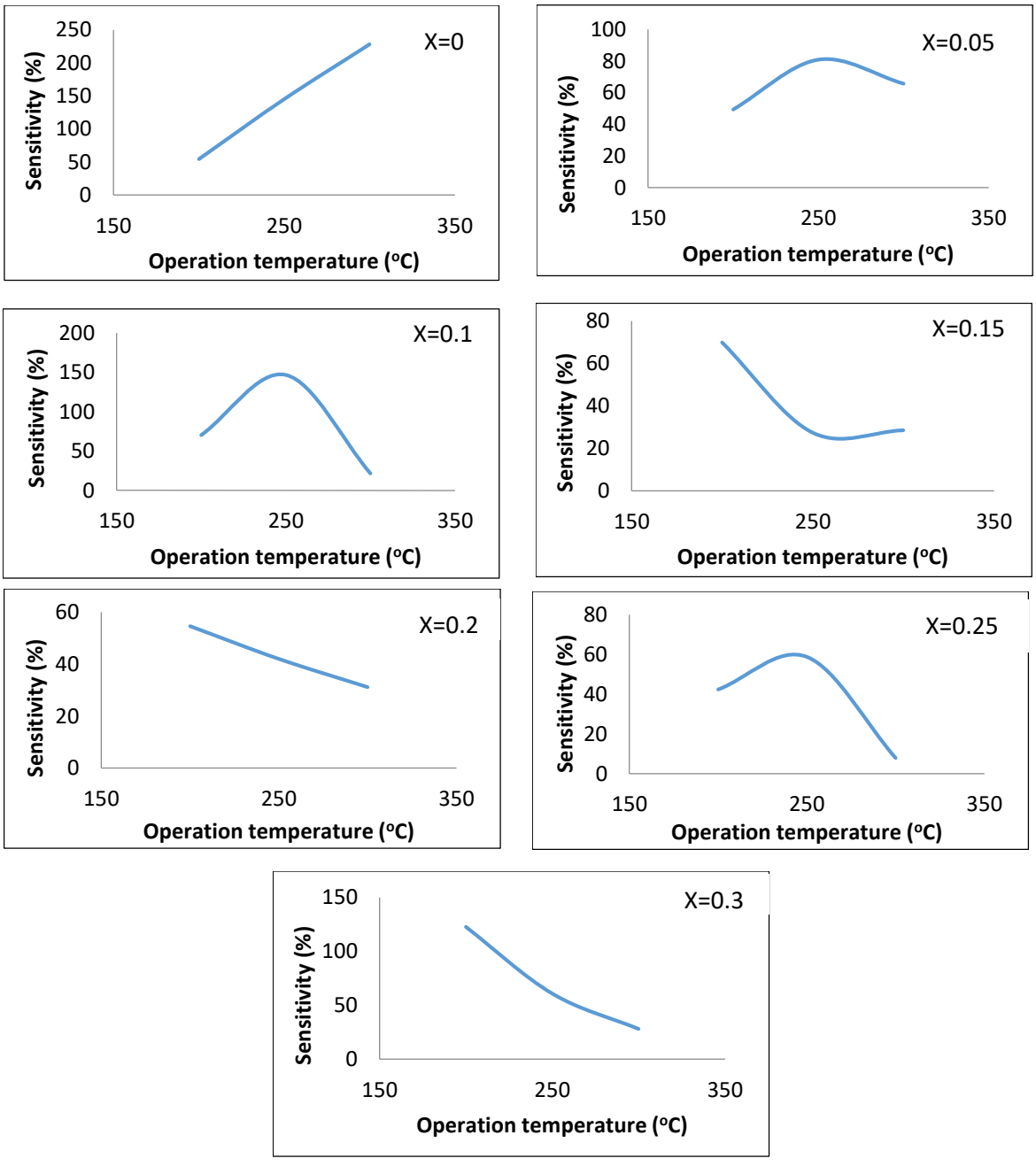

Figure 4. The sensitivity relationship to the operating temperature of the $Cu_xAl_{0.3-x}Ni_{0.7}Fe_2O_4$ samples.

Table (4) shows the highest sensitivity values for the samples of the prepared compound, and it is noted that the highest sensitivity value was at 250 ℃ when Cu Content is 0.10 mole.

Table 4. The highest sensitivity values of the H_2S gas for $Cu_xAl_{0.3-x}Ni_{0.7}Fe_2O_4$ Nanoparticles.

Cu Content (mole)	Operating temperature (℃)	Highest sensitivity value (%)
0.05	250	80.96118299
0.1	250	146.8493151
0.15	200	69.89247312
0.2	200	54.67349552
0.25	250	58.81612091
0.3	200	122.6415094

The sensitivity of $Cu_xAl_{0.3-x}Ni_{0.7}Fe_2O_4$ ferrite samples to the oxidizing gas hydrogen sulfide (H_2S) was studied. The samples reacted favorably to the aforementioned gas, allowing it to be used in a wide range of applications. The results showed that the ferrite nanocomposite $NiFe_2O_4$ activation process increases the value of the crystal lattice constant, resulting in a porous structure that increases the compound's specific surface area and, as a result, improves the sensor's sensitivity to the test gas [19]. When exposed to H_2S gas, the increase in free electrons may be responsible for the increase in sensor responsiveness. When the H_2S gas is removed, no more free electrons are produced, and the sensor is "washed" of H_2S gas, resulting in a reduction in both the number of free electrons and the electrical current signal. The H2S detecting technique is now reversible, which allows the sensor to be utilized for a variety of tests [6].

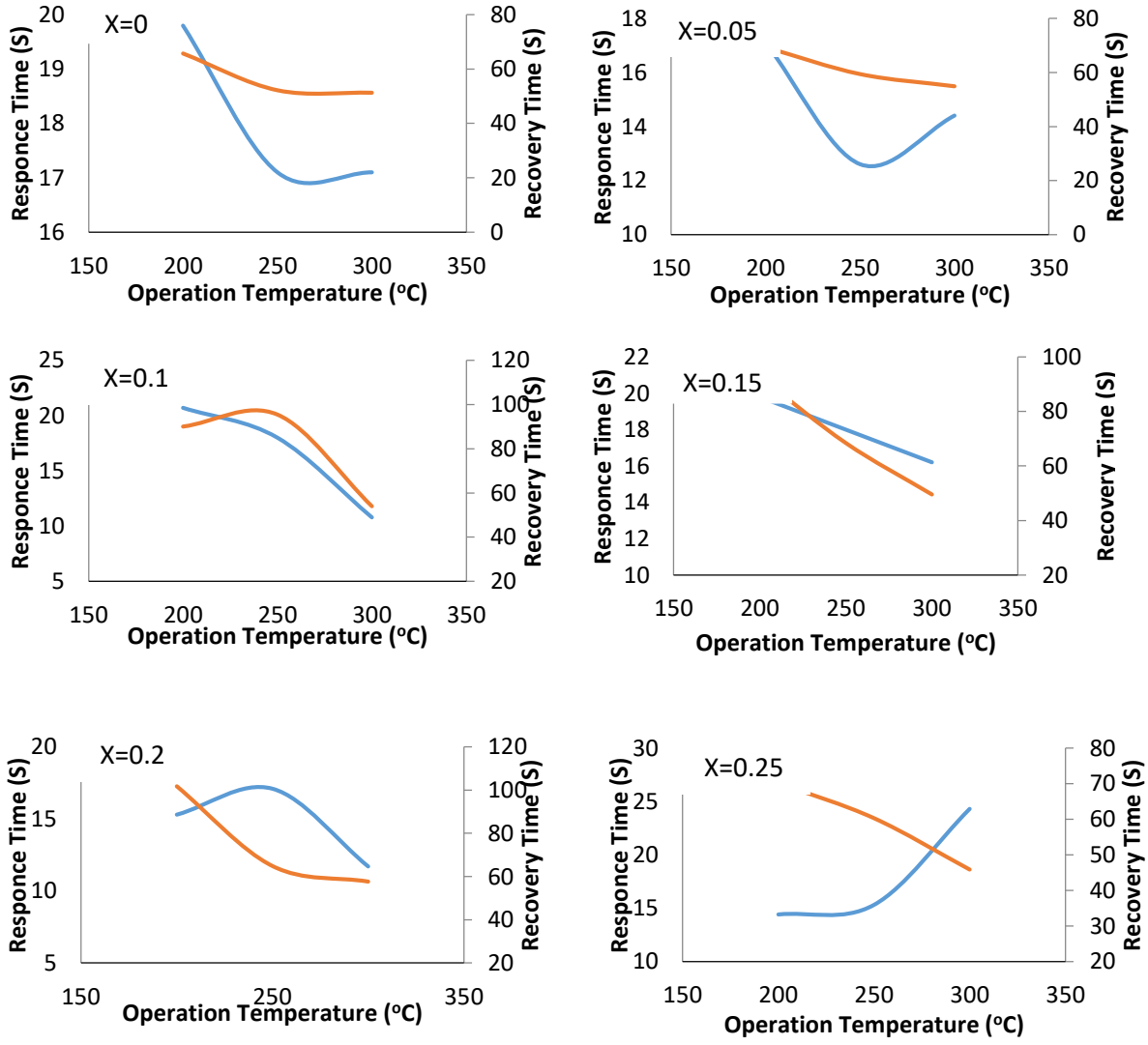

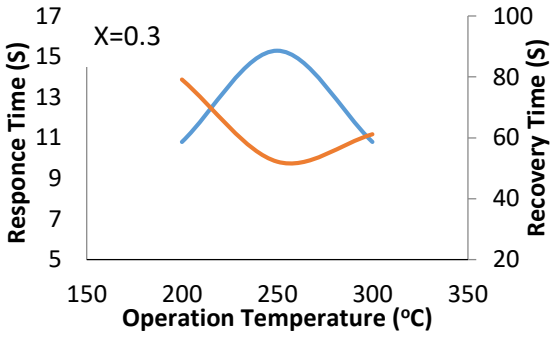

Figure 5. Relationship of response time and recovery time of H_2S gas at operatingtemperature for ferrite nanoparticles $Cu_xAl_{0.3-x}Ni_{0.7}Fe_2O_4$. Where the red line represents the response time, while the blue line represents the recovery time

Figure (5) shows that the addition of impurities in precise proportions to each new ion affects both the reaction time and the recovery time since these impurities impact the value of the lattice constant [20]. The speed of the interaction between oxygen atoms in the atmosphere and the gas atoms to be detected with atoms of the granular surface of the sensor material, as well as the geometric shape of the columns or electrodes, all influence the response time and recovery time. In return, these two factors depend on the operating temperature as an external, easily controlled factor and on the sample's composition [21]. The samples that best meet the necessary application are chosen since there are occasions when the same sample has a faster reaction and recovery time.

Table (5) shows that the minimum response time for H_2S gas for samples of the prepared compound was at an operating temperature of (200, 300) °C, while the minimum recovery time was at an operating temperature of 300° °C.

Table (5). Minimum response time and recovery time for $Cu_xAl_{0.3-x}Ni_{0.7}Fe_2O_4$ samples to H_2S gas.

Content (mole)	Minimum response time (sec)	Operating temperature (ºC)	Minimum recovery time (sec)	Operating temperature (ºC)
0	17.1	250,300	51.3	300
0.05	12.6	250	54.9	300
0.1	10.8	300	54	300
0.15	16.2	300	49.5	300
0.2	11.7	300	57.6	300
0.25	24.3	200	45.9	300
0.3	10.8	200,300	61.2	250

4. Conclusion:

The auto-combustion sol-gel technique was used to successfully synthesize ferrite single-phase nanoparticles containing nickel, aluminum, and copper ($Cu_xAl_{0.3-x}Ni_{0.7}Fe_2O_4$). The XRD and FE-SEM analyses for the samples of the synthesized chemical revealed that it is a ferrite nanoparticle of a type of spinel with a multi-crystalline face-centered cubic (FCC) structure, and it is of high purity, i.e. monophasic. This raised the compound's specific surface area, and doping the produced compound with aluminum enhanced the crystal lattice constant for this compound. The samples made of the nano ferrite demonstrated a good sensitivity to H_2S gas at various

operating temperatures. The samples recorded the highest sensitivity to it at the operating temperature of (250) ℃, and the minimum response time for the samples was at an operating temperature of (200, 300), while the minimum recovery time was at an operating temperature of 300 ℃.

References

1. Ghimbeu, C. M.; Lumbreras, M.; Siadat, M.; van Landschoot, R. C. ; Schoonman, J. Electrostatic sprayed SnO_2 and Cu-doped SnO_2 films for H2S detection. *Sensors and Actuators B: Chemical*, **2008**, *133*(2), 694-698.
2. Maekawa, T.; Tamaki, J.; Miura, N. ;Yamazoe, N.. Sensing behavior of CuO-loaded SnO_2 element for H2S detection. *Chemistry Letters*, **1991,** *20*(*4*), 575-578.
3. Devi, G. S.; Manorama, S., ; Rao, V. J. High sensitivity and selectivity of an SnO_2 sensor to H2S at around 100° C. *Sensors and Actuators B: Chemical*, **1995**,*28*(*1*), 31-37.
4. Tamaki, J.; Maekawa, T.; Miura, N. ; Yamazoe, N. CuO-SnO_2 element for highly sensitive and selective detection of H2S. *Sensors and Actuators B: Chemical*, **1992**, *9*(*3*), 197-203.
5. Wang, C.; Yin, L.; Zhang, L.; Xiang, D.; Gao, R. Metal oxide gas sensors: sensitivity and influencing factors. *sensors***,** **2010**, *10*(*3*), 2088-2106.
6. Ayesh, A. I.; Alyafei, A. A.; Anjum, R. S.; Mohamed, R. M.;Abuharb, M. B.; Salah, B.;El-Muraikhi, M. Production of sensitive gas sensors using CuO/SnO2 nanoparticles.. *Applied Physics A*, **2019**,*125*(8), 1-8.
7. Jain, A.; Baranwal, R. K.;Bharti, A.; Vakil, Z.;Prajapati, C. S. (2013). Study of Zn-Cu ferrite nanoparticles for LPG sensing. *The Scientific World Journal*, **2013**.
8. Laith Saheb1 , Tagreed, M. Al-Saadi Synthesis, Characterization, and NH_3 Sensing Properties of ($Zn_{0.7}$ $Mn_{0.3-x}$ Ce_x Fe_2O_4) Nano-Ferrite. *Journal of Physics: Conference Series*,**2021**,*2114*, 012040.
9. Ahmed, O. A.; Abed, A. H.; Al-Saadi, T. M. Magnetic Properties and Structural Analysis of Ce-Doped Mg–Cr Nano-Ferrites Synthesized Using Auto-Combustion Technique. In *Macromolecular Symposia*.**2022** *, 401, 1*, 2100311.
10. Tsvetkov, M.; Milanova, M.;Ivanova, I.; Neov, D.; Cherkezova-Zheleva, Z.; Zaharieva, J.; Abrashev, M. Phase composition and crystal structure determination of cobalt ferrite, modified with Ce, Nd and Dy ions by X-ray and neutron diffraction. *Journal of Molecular Structure*, **2019**,*1179*, 233-241.
11. Al-Saadi, T. M. ; Alsaady, L. J. Preparation of Silver Nanoparticles by Sol-Gel Method and Study their Characteristics. *Ibn AL-Haitham Journal For Pure and Applied Science*. **2015**, *28*(*1*).
12. Musa, K. H.; Al-Saadi, T. M. Investigating the Structural and Magnetic Properties of Nickel Oxide Nanoparticles Prepared by Precipitation Method. *Ibn Al-Haitham Journal For Pure and Applied Sciences*, **2022**, *35*(*4*).
13. Al-Saadi, T. M.; Abed, A. H.; Salih, A. A. Synthesis and Characterization of $Al_yCu_{0.15}Zn_{0.85-y}Fe_2O_4$ Ferrite Prepared by the Sol-Gel Method. *Int. J. Electrochem. Sci*, **2018**, *13*, 8295-8302.
14. Al-Saadi, T. M. ;Jihad, M. A. Preparation of graphene flakes and studying its structural properties. *Iraqi Journal of Science*, **2016**, *57*(*1*), 145-153.
15. Kumar, A.; Arora, M.; Yadav, M. S.; Panta, R. P. Induced size effect on Ni doped nickel zinc ferrite nanoparticles. *Physics Procedia*, **2010**, *9*, 20-23.
16. Jacob, B. P.; Thankachan, S.; Xavier, S.; Mohammed, E. M. Dielectric behavior and AC conductivity of Tb^{3+} doped $Ni_{0.4}Zn_{0.6}Fe_2O_4$ nanoparticles. *Journal of Alloys and Compounds*, **2012**, *541*, 29-35.

17. Hankare, P. P.;Vader, V. T.;Patil, N. M.; Jadhav, S. D.; Sankpal, U. B.;Kadam, M. R.; Gajbhiye, N. S. Synthesis, characterization and studies on magnetic and electrical properties of Mg ferrite with Cr substitution. *Materials Chemistry and Physics*, **2009**, *113*(*1*), 233-238.

18. Suryawanshi, S. S.; Deshpande, V. V.; Deshmukh, U. B.; Kabur, S. M.; Chaudhari, N. D.; Sawant, S. R. XRD analysis and bulk magnetic properties of Al3+ substituted Cu–Cd ferrites. *Materials chemistry and physics*, **1999**, *59*(3), 199-203.

19. Xuan, J.; Zhao, G.; Sun, M.; Jia, F., Wang, X.; Zhou, T. ; Liu, B. Low-temperature operating ZnO-based NO_2 sensors: a review. *RSC advances*, **2020**,*10*(65), 39786-39807.

20. Yahya, K. Characterization of Pure and Dopant TiO_2 Thin Films for Gas Sensors Applications, Doctoral dissertation, Ph. D Thesis, University of Technology Department of Applied Science, **2010**1-147.

21. Yüce, A.; Saruhan, B. 1.1. 3 Al-doped TiO_2 semiconductor gas sensor for NO_2-detection at elevated temperatures. Tagungsband, **2012**,68-71.